Rare Metal Materials and Engineering
Volume 50, Issue 2, February 2021
Available online at www.rmme.ac.cn

Science Press

Cite this article as: Rare Metal Materials and Engineering, 2021, 50(2): 0497-0503.

ARTICLE

Fabrication and Pore Structure of Directionally Solidified Porous Mg-Zn Alloy

Xiao Xinxiong[1,2], Liu Yuan[2,3], Jin Qinglin[1], Zhou Canxu[2], Zhang Huawei[2,3], Li Yan-xiang[2,3], Li Zaijiu[1]

[1] Faculty of Materials Science and Engineering, Kunming University of Science and Technology, Kunming 650093, China; [2] School of Materials Science and Engineering, Tsinghua University, Beijing 100084, China; [3] Key Laboratory for Advanced Materials Processing Technology, Ministry of Education, Tsinghua University, Beijing 100084, China

Abstract: Lotus-type porous Mg-Zn alloys were fabricated by the Bridgman-type directional solidification method. The pore structure and porosity of Mg alloys at different Zn contents and hydrogen pressures were studied. The porosity of Mg-1wt% Zn alloy was predicted through the theoretical calculation. The results show that pore structure can be influenced by the addition of Zn element. As the content of Zn increases from 0wt% to 2wt%, average pore diameter increases. The porosity of Mg-1wt% Zn alloy clearly decreases with increasing the hydrogen pressure from 0.1 MPa to 0.6 MPa. Based on a model for estimating the solubility of hydrogen in multi-component molten metals, the calculated results of porosity at the solidification stage (20 mm height) with a changed hydrogen pressure in Mg-1wt% Zn alloy are in good agreement with the experimental results. Through observations of the microstructures, the column grains of Mg-Zn alloy change into equiaxed grains as the content of Zn increases. Also, the formation of pore at different solidification stages was studied, which can supply theoretical basis for the fabrication of Gasar Mg-Zn alloy in the biomedical applications.

Key words: porous Mg-Zn alloy; Gasar process; directional solidification

Magnesium and its alloys are a perfect candidate for bone tissue engineering implants, due to their suitable mechanical properties and biocompatibilities properties[1]. Additionally, unlike conventional metal implants, such as titanium, stainless steel and cobalt-chromium, they are inert under physiological conditions. Magnesium and its alloys can be absorbed by human body. Hence, further surgery to remove the implant from human body can be avoided[1,2]. Porous Mg and its alloys maybe the potential candidates for bone tissue engineering application, exclusively at the load bearing area compared with the polymer or ceramic scaffolds, due to their good mechanical property and porous structure close to natural bone[3]. Furthermore, porous structure also facilitates bone ingrowth into the pores, which in turn facilitates stronger implant fixation at the initial stage of implantation. And, nutrient can be transferred faster and more efficiently through the pore channel, thus making them promising materials for bone tissue engineering applications[3,4].

In the last several decades, many methods have been developed to fabricate porous magnesium and its alloys, such as powder metallurgy[5,6] and infiltration process[7,8]. For biomedical application, the residual salt of infiltration process inside the porous materials may impair their biocompatibility. Based on the gas solubility gap between liquid and solid metals, regular porous metals with oriented long cylindrical pores can be prepared by directional solidification of molten metals saturated with hydrogen gas, which is called Gasar process[9-12]. Compared with the traditional fabrication process, the directional solidification process has many advantages, such as low cost, no contamination to melt, and tunable

Received date: February 25, 2020
Foundation item: National Natural Science Foundation of China (51771101)
Corresponding author: Liu Yuan, Ph. D., Professor, School of Materials Science and Engineering, Tsinghua University, Beijing 100084, P. R. China, E-mail: yuanliu@tsinghua.edu.cn

mechanical properties.

However, the clinical applications of porous Mg are restricted due to its faster degradation under physiological conditions, which intensely decreases the mechanical strength of the porous Mg and generates abundant hydrogen gas bubbles that prevent the surrounding tissues from healing[13,14]. With the purpose of searching for suitable alloying elements, Song[15] carried out the vitro corrosion tests for several magnesium alloys and pointed out that Ca, Mn and Zn can be appropriate candidates for biomedical magnesium alloys. Zinc is one of the most abundant essential elements in the human body[16], and has basic safety for biomedical applications. Furthermore, zinc can improve the corrosion resistance and mechanical properties of magnesium alloys. For instance, the corrosion rate of magnesium can be reduced by increasing the mass fraction of zinc in magnesium[17,18]. Besides, zinc can effectively strengthen magnesium[17,18] through a solid solution hardening mechanism[17]. Thus, the fabrication and research of directionally solidified porous Mg-Zn alloy can promote the application of porous magnesium alloy in medical fields.

1 Experiment

Gasar Mg-xZn(x=0, 1, 2, wt%) ingots were fabricated by Bridgman-type directional solidification method. The schematic drawing of experimental apparatus is shown in Fig.1. The furnace chamber is divided into a heating zone and a cooling zone by an adiabatic baffle. The heating zone is used to melt the Mg-Zn alloy and dissolve hydrogen. The cooling zone, composed of a vertical motion system controlled by a stepping motor and a copper chiller cooled with circulating water, is used for melt directional solidifying. Mg-xZn(x=0, 1, 2, wt%) alloy ingots were melted in the crucible (Fig.1a). In order to suppress the evaporation of magnesium during melting in vacuum, a small amount of hydrogen was introduced into the chamber before melting. After metals were melted, hydrogen gas with 99.99% purity was introduced into the chamber, and the temperature of the melt was monitored to 1023 K (750 °C) by a tungsten-rhenium thermocouple for 30 min to ensure hydrogen saturation in the melt. Afterwards, the turn-over plate is open and the copper chiller rises to touch the bottom of the graphite crucible. The graphite crucible with a certain withdrawing speed is then moved down from the hot zone to the cold zone through the pull rod (Fig.1b). The melt was directionally solidified upward from the water-cooled copper chiller. The hydrogen pressure was set at 0.1, 0.2, 0.4 and 0.6 MPa, separately, and the influence of hydrogen pressure and Zn concentration on porosity and pore size were investigated. The ingots were cut by a spark-erosion wire cutting machine parallel and perpendicular to the solidification direction. Each cross-section was polished with a series of silicon carbide sandpapers for pore morphology observation. The porosity and pore size were evaluated by an image analysis software. In order to observe the microstructure of

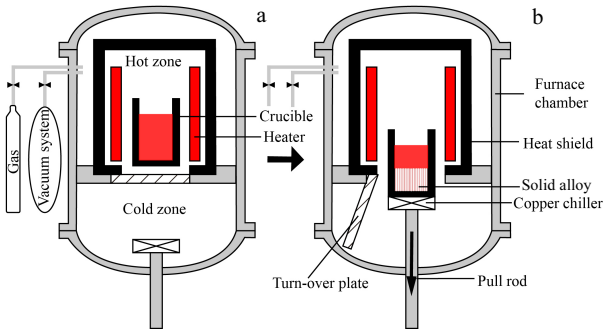

Fig.1 Schematic illustrations of the Bridgman-type directional solidification apparatus: (a) melting and holding process and (b) unidirectional solidification process

porous Mg-xZn(x=0, 1, 2, wt%) alloy ingots, the samples were sliced along the solidification direction at different heights. Grinding of the sliced samples was carried out on silicon carbide papers, followed by fine polishing with diamond (particle size from 2.5 to 0.5 μm). The samples were then subjected to ultrasonic cleaning in C_2H_5OH. The sample was etched in a solution of 1:20 with HNO_3:C_2H_5OH at room temperature. The corrosion sample was washed with C_2H_5OH and then dried. Finally, the microstructure of the specimens was examined by an optical microscope (Carl Zeiss AG, Germany).

2 Results and Discussion

2.1 Characterization of pore morphology and structure parameter

Fig.2 shows the effect of increasing the zinc content on the pore morphology of directionally solidified porous Mg-xZn (x=0, 1, 2, wt%) alloy when the hydrogen pressure is 0.2 MPa. Fig.2 indicates that the pore structure of the ingot changes significantly with increasing the zinc content. Comparing the longitudinal sectional views of three ingots with different zinc contents, as the zinc content increases, the stability of the pores becomes worse, the pore diameter becomes larger, and the inner wall of the pores gradually becomes rough. Fig.2a shows the directional solidification of porous pure magnesium. Combining the longitudinal section and the cross section at different solidification heights, it can be found that the increase in solidification height does not have much effect on its pore morphology. Fig.2b and 2c are directionally solidified porous magnesium-zinc alloys. It can be found that non-directional pores appear in the upper part of the ingot after the zinc element is added. And with the increase of zinc content, when the solidification height is greater than 60 mm, the non-directional pores increase significantly. At the same time, the addition of alloying elements also changes the pore size greatly with the increase of solidification height. This change is most vividly shown in Fig.2c. When the solidification height

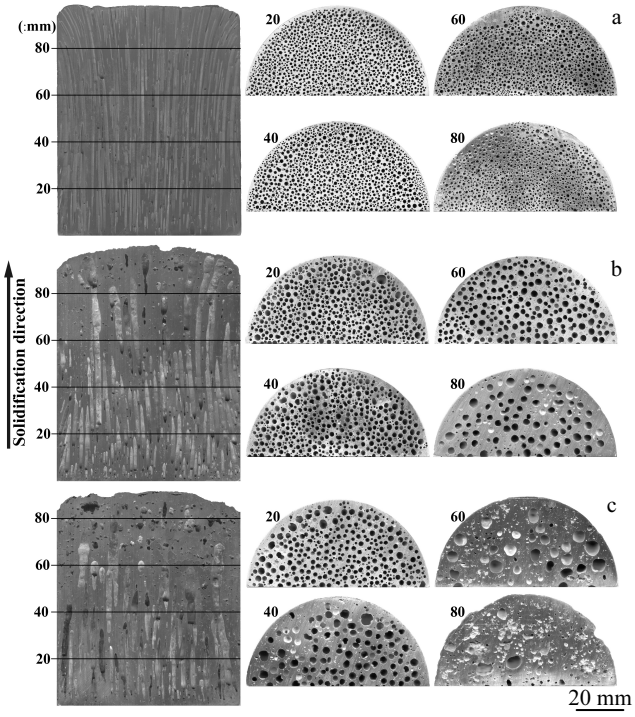

Fig.2 Influence of Zn concentration of Mg-*x*Zn(*x*=0, 1, 2, wt%) alloys on pore morphology under the hydrogen pressure of 0.2 MPa: (a) *x*=0wt%, (b) *x*=1wt%, and (c) *x*=2wt%

is 20 mm, there are hundreds of directional pores; when the solidification height is 80 mm, there are only a few directional pores.

Fig.3 shows the effect of hydrogen pressure on the pore morphology of directionally solidified porous Mg-1Zn alloy. It can be clearly seen from the longitudinal section of the ingot that both the pore size and the overall porosity decrease with increasing the hydrogen pressure. And the number of directional pores in the lower half of the ingot is significantly higher than that in the upper half; the upper half is replaced by many non-directional pores. The pore wall of the upper half of the ingot is obviously rougher than that of the lower half. In addition, with the increase of hydrogen pressure, non-directional pores appear earlier in the solidification process of the ingot.

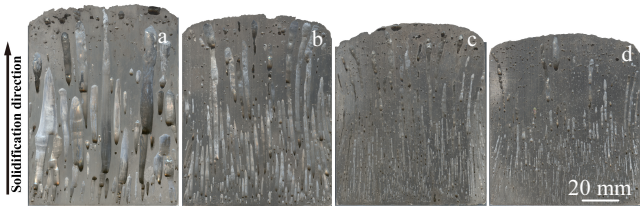

Fig.3 Influence of hydrogen pressure on pore morphology of Mg-1%Zn alloy: (a) 0.1 MPa, (b) 0.2 MPa, (c) 0.4 MPa, and (d) 0.6 MPa

The above phenomena show that the increase of hydrogen pressure and solidification height are not conducive to the stable growth of pores. This result deviates from the directional solidification of porous pure metals.

Fig.4 shows the average pore diameter and porosity in the cross section of the ingot at different heights under the hydrogen pressure of 0.2 MPa. It can be clearly found that the average pore diameter and surface porosity of directionally solidified porous pure magnesium do not fluctuate much with the change of solidification height. With the addition of alloy elements, the average pore diameter increases with increasing the solidification height, while the surface porosity shows the opposite trend. The variation of the average pore diameter and the surface porosity deviation of the same ingot with the height even reaches two to three times. The variation of pore parameters between different ingots shows an increasing trend with the change of height. In addition, the higher the alloying element content, the greater the variation of the pore parameter deviation with the solidification height.

The effect of hydrogen pressure on the pore structural parameters of directionally solidified porous Mg-1Zn alloy is shown in Fig.5. The average pore diameter basically decreases when hydrogen pressure increases from 0.1 to 0.6 MPa at the same solidification height. And the average pore diameters of Mg-1Zn alloy vary greatly with the increase of solidification heights. As the solidification height increases, the porosity

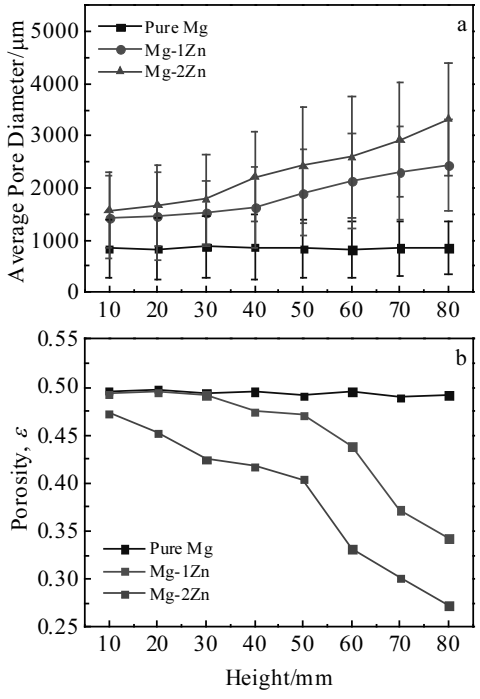

Fig.4 Average pore diameter (a) and porosity, ε (b) of Mg-*x*Zn (*x*=0, 1, 2, wt%) alloys on the cross section at different heights under the hydrogen pressure of 0.2 MPa

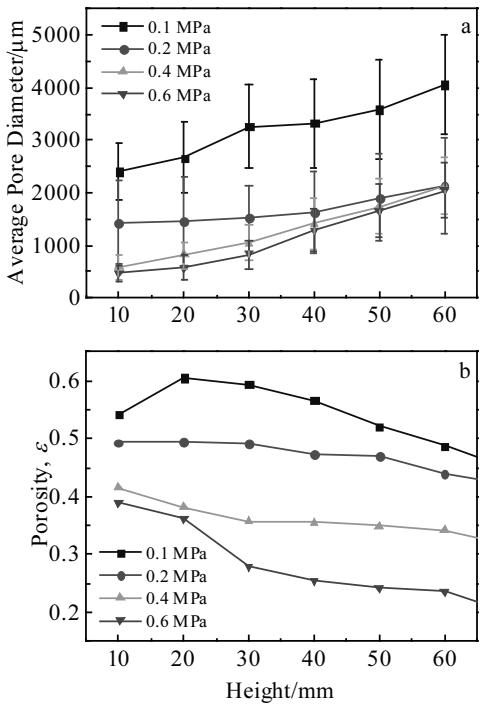

Fig.5 Average pore diameter (a) and porosity, ε (b) of Mg-1Zn alloy at different heights under different hydrogen pressures

ranges from 0.604 to 0.487 at hydrogen pressure of 0.1 MPa, 0.494 to 0.438 at hydrogen pressure of 0.2 MPa, 0.415 to 0.342 at hydrogen pressure of 0.4 MPa, and 0.388 to 0.235 at hydrogen pressure of 0.6 MPa. Porosity fluctuates little with height under the hydrogen pressure of 0.2 and 0.4 MPa. On the contrary, when hydrogen pressure is 0.1 and 0.6 MPa, its porosity fluctuates greatly with solidification heights. And directionally solidified porous Mg-Zn alloy should have a pore diameter suitable for its stable growth.

2.2 Prediction porosity of Mg-1Zn alloy under different H_2 pressure

It is well known that porosity is an important parameter for porous materials. The porosity of the directionally solidified porous metal is closely related to the hydrogen pressure. Liu et al[19] established a theoretical model and successfully predicted the porosity of pure Mg, and the model is shown in the following formula:

$$\varepsilon = \frac{[C_0(1-a)\rho_s - \overline{C}_s\rho_L]RT_m}{[C_0(1-a)\rho_s - \overline{C}_s\rho_L]RT_m + p_{pore}\cdot\rho_L} \quad (1)$$

where ε is the theoretical overall porosity, R is the gas constant, T_m is the melting point of the metal, ρ_s is the density (kg/m^3) of the solid metal and p_{pore} is the gas pressure (Pa) in the pore which is almost equal to the furnace atmosphere, C_0 is the initial hydrogen concentration in the liquid metal (mol/m^3), $\overline{C}_s$ is the hydrogen concentration in the solid metal, ρ_L is the density of solid metal near the melting point, a is an escape coefficient which is equal to the ratio of the escaping hydrogen to the original hydrogen concentration in the liquid metal. In this paper, C_0 and $\overline{C}_s$ are the initial hydrogen concentration in the liquid and solid Mg-1Zn alloy, respectively. And the mole fraction x_H of hydrogen in the alloy can be solved via the following equation[20]:

$$\ln x_H = \sum_i x_i \ln x_{H,i} + \Delta G_m^{ex}/RT \quad (2)$$

where x_H is the mole fraction of the hydrogen in the alloy, x_i is the mole fraction of alloying element i in the alloy, $x_{H,i}$ is the mole fraction of the hydrogen in the pure element i, ΔG_m^{ex} is the excess molar Gibbs free energy. The solubility of hydrogen in the liquid and solid pure element Mg/Zn is calculated by the following equation[21]:

$$\ln S_{H,Mg} = 6.558 - \frac{2533}{T} + \frac{1}{2}\ln\left(\frac{p_H}{p_0}\right) \quad \text{Liquid} \quad (3)$$

$$\ln S_{H,Mg} = 5.701 - \frac{2210}{T} + \frac{1}{2}\ln\left(\frac{p_H}{p_0}\right) \quad \text{Solid} \quad (4)$$

And ΔG_m^{ex} can be expressed as follows:

$$\Delta G_m^{ex} = \Delta H_m - T\Delta S_m^{ex} \quad (5)$$

Based on the Miedema mixed heat model, the mixture heat ΔH_m of binary alloy can be represented as[22,23]:

$$\Delta H_m = f(x_i,V)\cdot g(x_i,n_{ws})p\left[\frac{q}{p}\left(\Delta n_{ws}^{1/3}\right)^2 - (\Delta\phi)^2 - \frac{r}{p}\right] \quad (6)$$

$$f(x_i,V) = \frac{x_i x_j V_{i,m}^{2/3} j_{j,m}^{2/3}}{\left(x_i V_{i,m}^{2/3} + x_j j_{j,m}^{2/3}\right)^2} \quad (7)$$

$$g(x_i,n_{ws}) = 2\frac{x_i V_{i,m}^{2/3} + x_j j_{j,m}^{2/3}}{\left(n_{ws}^{1/3}\right)_i + \left(n_{ws}^{1/3}\right)_j} \quad (8)$$

where $V_{i,m}$ and $V_{j,m}$ are the molar volume (m^3/mol) of alloy elements i and j in alloys, respectively. With valence of metal elements, molar volume V_i under the pure state and electronegativity ϕ have the following relationship:

$$V_{i,m}^{2/3} = V_i^{2/3}[1 + \mu_i x_i(\phi_i - \phi_j)] \quad (9)$$

where μ_i is a constant related to valence: μ_j is 0.14 (univalent alkali metals), 0.10 (divalent alkali metals), 0.07 (trivalent primary metals and precious metals), and 0.04 (other metals). The q/p is 9.4

The molar surplus entropy ΔS_m^{ex} of binary alloy can be expressed as the function of mixed heat ΔH_m using the approximate formula proposed by Tanaka[24-26]:

$$\begin{cases} \Delta S_m^{ex} = \dfrac{1}{14.0}\Delta H_m\cdot(1/T_{m,i} + 1/T_{m,j}) & \text{Liquid} \\ \Delta S_m^{ex} = \dfrac{1}{15.1}\Delta H_m\cdot(1/T_{m,i} + 1/T_{m,j}) & \text{Solid solution} \end{cases} \quad (10)$$

The density of the Mg-1%Zn alloy is calculated by linear adding principle. The values of relevant parameters are shown

in Table 1. And the theoretically predicted porosity of Mg-1%Zn alloy agrees with the porosity at 20 mm of the ingot solidification height and differs greatly from the overall porosity, as shown in Table 2. This is mainly due to the increase in the width of the mushy zone at the front of the solid-liquid interface as the solidification height increases.

2.3 Influence of solidification mode on pore morphology

The pore structure of directionally solidified porous alloys is directly affected by the solidification mode. For pure metal, the supercooling degree at the front of solid-liquid interface is small, and the solidification mode is mainly at the flat interface. The gas-solid phase grows cooperatively, and the pore distribution is relatively uniform. However, for alloy, there is a mushy zone at the front of the solid-liquid interface, which makes the solid-liquid interface tend to be unstable. Jiang et al[27] found that the deterioration and interruption of the directional pore structure is related to the change of the solidification mode of the alloy. According to the different solid-liquid interface, the solidification modes of the alloy can be divided into four types: plane solidification, cellular solidification, columnar dendrite solidification and equiaxial dendrite solidification, which results in four kinds of microstructure. The microstructure of the longitudinal sections of Mg-*x*Zn (*x*=0, 1, 2, wt%) alloy at different heights is shown in Fig.6. The directionally solidified porous pure Mg has coarse regular columnar grains throughout the solidification process, which also makes it presents a regular cylindrical pore. The microstructure of the Mg-1Zn is fine columnar crystals at a height of 0 mm to 40 mm, equiaxial dendritic structures appear at the height from 40 mm to 60 mm, and finally they all transform to equiaxial dendritic structure at a height of 60 mm. This microstructure determines that the pores in the lower part are well oriented and the pores in the upper part are poorly oriented. The microstructure of the Mg-2Zn is equiaxed dendrite throughout the solidification process. And as the solidification height increases, the grains

Table 1 Miedema model parameter values[22]

Element	ϕ/V	$n_{ws}^{1/3}$ / *d.u.*$^{-1}$	$V^{2/3}$/cm^2	r/p^*	r/p type
Mg	3.45	1.17	5.8	0.4	b
Zn	4.10	1.32	4.4	1.4	b

* For solid alloys, the r/p equals 0 when the r/p types of the two alloy elements are the same; for liquid alloys, multiply the calculated value by 0.73

Table 2 Comparisons between the calculated and experimental porosity of Mg-1Zn alloy

Hydrogen pressure/MPa	Melting temperature/K	Overall porosity, ε	Porosity at 20 mm height	Calculated porosity, ε
0.1	1023	0.455	0.604	0.611
0.2	1023	0.421	0.494	0.514
0.4	1023	0.376	0.382	0.399
0.6	1023	0.347	0.361	0.374

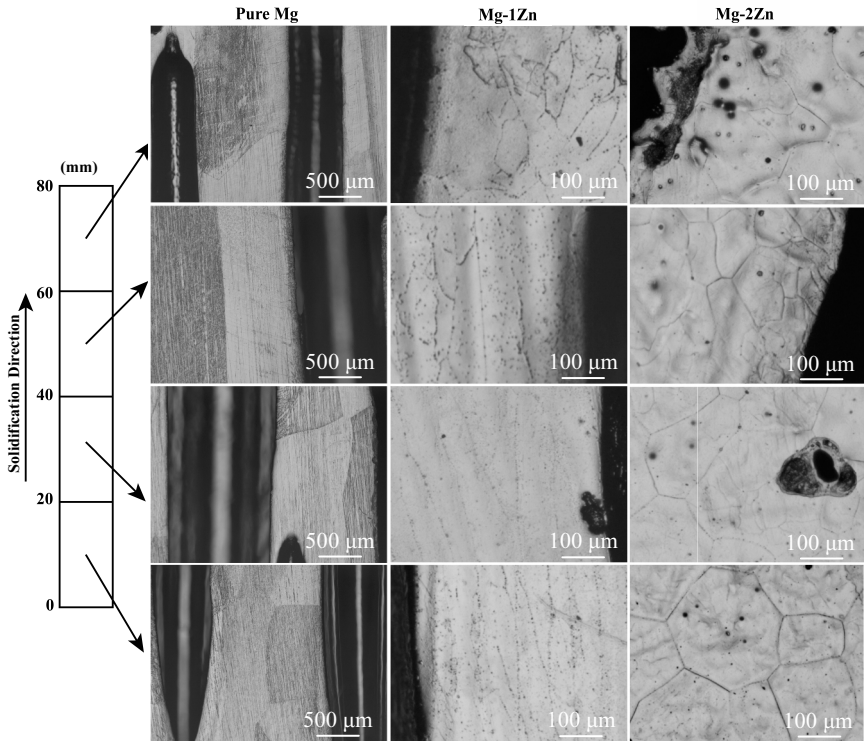

Fig.6 Microstructures of Mg-*x*Zn (*x*=0, 1, 2, wt%) alloy at different heights

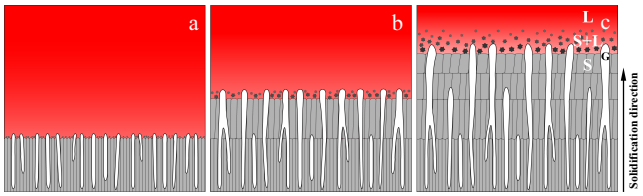

Fig.7 Schematic illustration of the effect of the width in the mushy zone on the pore growth

gradually become finer. These results can be explained by changes in the width of the solid-liquid coexistence zone. For preparing directionally solidified porous magnesium alloys, Hoshiyama et al.[28] found that as the content of alloy elements increases, the temperature range of the solid-liquid phase of the alloy increases, and the mushy zone at the front of the solid-liquid interface is expanded, making it difficult to obtain the directional pore structure. A schematic drawing of the effect of the width of solid/liquid coexistence region on the pore growth is shown in Fig.7. At the initial stage of solidification, the temperature gradient at the front of the solid-liquid interface is large, and the sample can be solidified in cellular structure. As the solidification proceeds, the temperature gradient gradually decreases, causing the decrement of solidification rate and the pore becomes larger. Under the dual action of solidification rate and solute redistribution, the mushy zone gradually is widened, which seriously affects the grain orientation and the direction of the pores. The instability of the pores causes many pore coalescence. These factors cause shorter columnar crystals which eventually transform into equiaxial crystal structures. When the width of the mushy zone is much larger than the pore diameter, the pores are gradually interrupted. However, there are still some columnar pores that have grown in the equiaxed crystal regions for a while, as show in Fig.2 and Fig.6.

3 Conclusions

1) As the content of Zn increases, average pore diameter at the same height of the ingots increases. And as the content of Zn increases, the orientation of pores becomes worse and non-directional pores increase.

2) Porosity of Mg-1Zn alloy decreases with increasing the H_2 pressure. The increment of the H_2 pressure can decrease the pore diameters of Mg-Zn alloy at the same ingot height.

3) Based on a model for estimating the solubility of hydrogen in multi-component molten metals, the calculated results of porosity at the solidification stage (20 mm height) in Mg-1Zn alloy with the change of hydrogen pressure are in good agreement with the experimental result.

4) Through observations on the microstructures, results show that the column grains of Mg-Zn alloy change into equiaxed grains as the content of Zn increases. At the initial solidification stage, the increment of width of mushy zone can weaken the ability of orientation of fine directional pores, which can lead to the pore coalescence. And at the middle stage, large pores are more stable and retained. At the final stage, the width of mushy zone is larger than the pore diameters, which can interrupt the growth of the pore, and many unidirectional pores form.

References

1 Staiger M P, Pietak A M, Huadmai J. *Biomaterials*[J], 2006, 27(9): 1728
2 Hornberger H, Virtanen S, Boccaccini A R. *Acta Biomaterialia*[J], 2012, 8(7): 2442
3 Blaker J J, Maquet V, Jérôme R. *Acta Biomaterialia*[J], 2005, 1(6): 643
4 Battiston K G, Cheung J W C, Jain D. *Biomaterials*[J], 2014, 35(15): 4465
5 Wen C E, Mabuchi M, Yamada Y. *Scripta Materialia*[J], 2001, 45(10): 1147
6 Kang M H, Lee H, Jang T S. *Acta Biomaterialia*[J], 2019, 84: 453
7 Yamada Y, Shimojima K, Sakaguchi Y. *Journal of Materials Science Letters*[J], 1999, 18(18): 1477
8 Gaozhi J, Chenxin C, Jian Z. *Corrosion Science*[J], 2018, 144: 301
9 Shapovalov V. *USA Patent*, 5181549[P], 1993
10 Liu Yuan, Li Yanxiang. *Transactions of Nonferrous Metals Society of China*[J], 2003, 13(4): 830
11 Liu Yuan, Li Yanxiang, Zhang Huawei *et al*. *Rare Metal Materials and Engineering*[J], 2005, 34(7): 1128 (in Chinese)
12 Liu Yuan, Li Yanxiang. *Acta Metallurgica Sinica*[J], 2010, 46(2): 129 (in Chinese)
13 Gu X N, Zhou W R, Zheng Y F. *Materials Letters*[J], 2010, 64(17): 1871
14 Zeng R, Dietzel W, Witte F. *Advanced Engineering Materials*[J], 2008, 10(8): 3
15 Song G. *Corrosion Science*[J], 2007, 49(4): 1696
16 Tapiero H, Tew K D. *Biomedicine & Pharmacotherapy*[J], 2003, 57(9): 399
17 Zhang S, Zhang X, Zhao C. *Acta Biomaterialia*[J], 2010, 6(2): 626
18 Kainer K U. *Magnesium-Alloys and Technology*[M]. Weinheim: Wiley-Vch Gmbh & Co, 2003: 226
19 Liu Yuan, Li Yanxiang, Wan Jiang. *Materials Science and Engineering A*[J], 2005, 402(1-2): 47
20 Jiang G R. *Study on Hydrogen Solubility in Molten Alloys and Directional Solidification of Porous Cu-Mn Alloy*[D]. Beijing: Tsinghua University, 2010 (in Chinese)
21 Zhang Huawei, Li Yanxiang, Liu Yuan. *Acta Metallurgica Sinica*[J], 2007, 43(2):113 (in Chinese)
22 Miedema A R, De Chatel P F, De Boer F R. *Physica B+c*[J], 1980, 100(1): 1
23 Niessen A K, De Boer F R, Boom R D. *Calphad*[J], 1983, 7(1): 51
24 Tanaka T, Gokcen N A, Morita Z I. *Zeitschrift für Metallkunde*[J],

1993, 84(3): 192
25 Tanaka T, Gokcen N, Morita Z. *Zeitschrift für Metallkunde*[J], 1990, 81(5): 349
26 Tanaka T, Gokcen N A, Morita Z. *Zeitschrift für Metallkunde*[J], 1990, 81(1): 49
27 Jiang G R, Li Yanxiang, Liu Yuan. *Transactions of Nonferrous Metals Society of China*[J], 2011, 21(1): 88
28 Hoshiyama H, Ikeda T, Nakajima H. *High Temperature Materials and Processes*[J], 2007, 26(4): 303

定向凝固多孔 Mg-Zn 合金的制备及气孔结构

肖心雄[1,2]，刘　源[2,3]，金青林[1]，周灿旭[2]，张华伟[2,3]，李言祥[2,3]，李再久[1]
(1. 昆明理工大学 材料科学与工程学院，云南 昆明 650093)
(2. 清华大学 材料科学与工程学院，北京 100084)
(3. 先进成形制造教育部重点实验室（清华大学），北京 100084)

摘　要：采用 Bridgman 型定向凝固法制备出藕状多孔 Mg-Zn 合金。研究了不同锌含量和氢气压力对气孔形貌的影响。通过理论计算对 Mg-1Zn（质量分数，%，下同）合金的孔隙率进行了预测。结果表明，锌元素的加入会对孔结构产生重大影响。随着 Zn 含量从 0%增加到 2%，平均孔径增加。随着氢气压力从 0.1 MPa 增加到 0.6 MPa，Mg-1Zn 合金的孔隙率明显降低。基于氢气在多组分熔融金属中溶解度的计算模型，Mg-1Zn 合金铸锭凝固高度为 20 mm 的不同氢压孔隙率的计算结果与实验的结果比较吻合。通过组织观察表明，随着 Zn 含量的增加，凝固组织由柱状晶转变为等轴晶。此外，研究了在不同凝固阶段孔的形成过程，可为在生物医用材料中应用的定向凝固多孔 Mg-Zn 合金的制备提供理论依据。

关键词：多孔镁锌合金；Gasar 工艺；定向凝固

作者简介：肖心雄，男，1993 年生，硕士，昆明理工大学材料科学与工程学院，云南 昆明 650093，E-mail: 1072514928@qq.com